Inorg. Chem. **2003**, *42*, 7207–7218

Inorganic Chemistry
Article

Comparison of M–S, M–O, and M-(η^2–SO) Structures and Bond Dissociation Energies in d^6 $(CO)_5M(SO_2)^{nq}$ Complexes Using Density Functional Theory

Heather J. Retzer and Thomas M. Gilbert*,[1]

Department of Chemistry and Biochemistry, Northern Illinois University, DeKalb, Illinois 60115

Received June 3, 2003

Density functional theory studies of the series of isomeric d^6 (pentacarbonyl)metal complexes $(CO)_5M(\eta^1\text{-}SO_2)^{nq}$, $(CO)_5M(\eta^1\text{-}OSO)^{nq}$, and $(CO)_5M(\eta^2\text{-}SO_2)^{nq}$ (M = Ti–Hf, nq = 2–; M = V–Ta, nq = 1–; M = Cr –W, nq = 0; M = Mn–Re, nq = 1+; M = Fe–Os, nq = 2+) provide accurate structural modeling and quantitative prediction of the relative stabilities of the isomers. The η^1-S-bound complexes display planar SO_2 moieties that adopt staggered orientations with respect to the carbonyl ligands, in keeping with experimental observations. The OSO chain in the η^1-O-bound complexes generally adopts the u-shape with a staggered orientation. The dianions $(CO)_5(Ti\text{–}Hf)(\eta^1\text{-}OSO)^{2-}$ differ in that the OSO chain adopts the eclipsed z-shape orientation. The η^2-SO_2 complexes exhibit a facial interaction and are stable only for anionic and neutral complexes, supporting the view that this motif involves substantial M → SO_2 π-back-bonding. The relative stabilities of the isomers generally follow u-shaped trends both across a row and down a family. This fits with qualitative ideas that the bond dissociation energies (BDEs) for the $(CO)_5M(SO_2)^{nq}$ complexes track competition between relative hardness/softness of the metal fragment and its capacity for π-back-bonding. Quantitatively, examination of BDEs by bond energy decomposition approaches suggests that electrostatic considerations dominate bonding for the η^1-SO_2 complexes and covalent effects dominate for the η^2-SO_2 species, while both are important for η^1-OSO complexes.

Introduction

Sulfur dioxide, SO_2, has long been recognized as a polluting product of coal and natural gas combustion. It acts as a respiratory irritant at concentrations as low as 2 ppm,[2] and it oxidizes slowly in air to sulfur trioxide, SO_3, a major contributor to acid rain. Minimizing or eliminating sulfur dioxide emissions represents a worthy socioeconomic goal.

The need for catalysts designed to convert SO_2 to less hazardous materials has driven the study of its coordination to transition metal fragments and subsequent reactivity. Several efforts here have shown links between coordination mode and further reactivity. For example, $(Ph_3P)_3Pt(\eta^1$-pyramidal S-bonded $SO_2)$ reacts with molecular oxygen to form $(Ph_3P)_3Pt(SO_4)$,[3] while $(Ph_3P)_3Ni(\eta^1$-nearly planar S-bonded $SO_2)$ does not.[4] Consequently, syntheses designed to form SO_2 complexes exhibiting all of the possible bonding motifs to a single transition metal have appeared. Of the possible motifs including η^1-planar-S-bonded, η^1-pyramidal-S-bonded, various η^1-O-bonded, and η^2-SO-bonded SO_2 (Scheme 1), examples exist of several. Qualitative and semiquantitative models exist to predict what bonding mode a particular metal fragment will prefer.[5] However, little work

Scheme 1

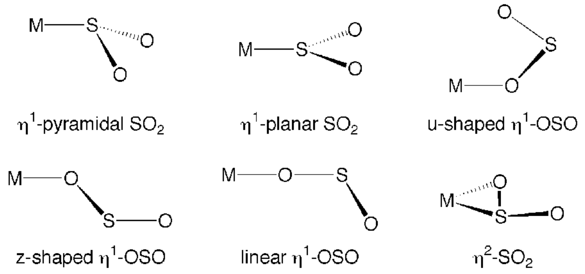

---

(1) Correspondence to this author at Northern Illinois University. E-mail: tgilbert@marilyn.chem.niu.edu.

(2) Weil, E. D.; Sandler, S. R. Sulfur Compounds. In *Kirk-Othmer Encyclopedia of Chemical Technology*, 4th ed.; Wiley: New York, 1994; Vol. 23, pp 299−340.

(3) Levison, J. J.; Robinson, S. D. *J. Chem. Soc., Dalton Trans.* **1972**, 2013−2017.

(4) Moody, D. C.; Ryan, R. R. *Inorg. Chem.* **1979**, *18*, 223−227.

(5) Ryan, R. R.; Kubas, G. J.; Moody, D. C.; Eller, P G. *Struct. Bonding* **1981**, *46*, 47−100.

10.1021/ic030179p CCC: $25.00

has focused on directly measuring the thermodynamics of SO_2 bonding,[6,7] or quantitatively explaining trends in structural or stability behavior. We have minimal detailed knowledge of the fundamental issues, such as the relative energies of the various SO_2 bonding configurations.

We have begun to address this lack computationally, modeling the structures and reactions of an array of transition metal−SO_2 complexes. We believe the work will provide fundamental data regarding metal−S and metal−O bond strengths, which will then give insight into bonding theories and their application. Furthermore, the results should suggest preferred routes and catalysts for desired conversions of SO_2. We report here our initial studies, involving the structures and relative bond dissociation energies (BDEs) of the series of isomeric d^6 (pentacarbonyl)metal complexes $(CO)_5M(\eta^1\text{-}SO_2)^{nq}$, $(CO)_5M(\eta^1\text{-}OSO)^{nq}$, and $(CO)_5M(\eta^2\text{-}SO_2)^{nq}$ ($M =$ Ti−Hf, $nq = 2-$; $M =$ V−Ta, $nq = 1-$; $M =$ Cr−W, $nq = 0$; $M =$ Mn−Re, $nq = 1+$; $M =$ Fe−Os, $nq = 2+$). While only $(CO)_5Cr(\eta^1\text{-planar-}SO_2)$ has been structurally characterized,[8] members of the monoanionic,[9] neutral,[10] and monocationic[11] classes have been prepared and characterized by other means. We thus have bases for comparisons between experimental and computational results. Moreover, the d^6 $(CO)_5M$ fragment is well-studied and understood, so the complexes should provide readily interpreted bonding features and energies.

Computational Details

All DFT calculations were carried out using the Amsterdam Density Functional (ADF 2002) program[12] developed by Baerends et al.[13] and vectorized by Ravenek.[14] The numerical integration scheme applied for the calculations was developed by te Velde et al.;[15] the geometry optimization procedure was based on the method of Versluis and Ziegler.[16] Geometry optimizations used the local density approximation of Vosko, Wilk, and Nusair (LDA VWN)[17] augmented with the nonlocal gradient correction PW91 from Perdew and Wang.[18] Test calculations using other gradient corrections such as BP86 or revPBE gave essentially identical BDEs for several compounds. Relativistic corrections were added using the zeroth order relativistic approximation (ZORA) approach.[19] The electronic configurations of the molecular systems were described by a triple-ζ basis set for all atoms, with polarization functions on C, O, and S (the TZP basis set in ADF). All atoms were assigned a relativistic frozen core potential, treating as core the shells up to and including the following: 1s for C, N, and O, 2p for first-row transition metals and S, 3d for second-row metals, and 4d for third-row metals. A set of auxiliary s, p, d, and f functions, centered on all nuclei, was used to fit the molecular density and represent Coulomb and exchange potentials accurately in each SCF cycle.[20]

For each molecule/ion, a systematic variety of starting geometries were optimized without constraints to span the possible conformational spaces and ensure that a global minimum was located. For example, for all $(CO)_5M(OSO)^{nq}$ complexes, four starting geometries were each optimized to a stationary point, each geometry being a combination of the z or u OSO chain conformations and the staggered or eclipsed orientations with respect to the carbonyl ligands. Once an optimized minimum structure was obtained, single point energies using a spin−orbit ZORA relativistic Hamiltonian were calculated for the $(CO)_5M(SO_2)^{nq}$ complex and for the separately optimized $(CO)_5M^{nq}$ fragment. Subtraction of the latter plus the single point spin−orbit relativistic energy of SO_2 from the former gave the bond dissociation energies (BDEs) reported in Table 4. The data were not corrected for basis set superposition error (BSSE), because the correction at this basis set level is probably ≤ 2.0 kcal mol^{-1} [21] and because it is probably systematic across the series of molecules investigated and, thus, will not affect trend comparisons. Also, because of the number of molecules investigated and the computational effort required to calculate second derivatives of the energy with respect to the nuclei positions (the ADF program does this through laborious numerical integration), we did not calculate Hessian matrices for every complex to confirm that the structures determined exhibited only positive frequencies. Because of this limitation, the energy data are not corrected for zero point vibrational energy (ZPE). This correction is generally small due to its near cancellation in the reaction energy calculation. To support this, we calculated the ZPE correction for the reaction $(CO)_5Mo(\eta^1\text{-}SO_2) \rightarrow (CO)_5Mo + SO_2$, finding a value of 1.2 kcal mol^{-1}. Frequency calculations were performed only for those (pentacarbonyl)metal systems for which experimental IR vibrational spectra have appeared in the literature. All of them exhibited only positive frequencies, indicating that they are true minima.

As the calculated structures typically exhibit expected bond distances and angles, particularly for the carbonyl ligands, only notable parameters appear in the following text. Optimized Cartesian coordinates of all molecules discussed are available as Supporting Information.

---

(6) A substantial number of studies have focused on the thermochemistry of SO_2 with gas-phase transition metal atoms, and with solid surfaces. For the former, see: (a) McClean, R. E. *J. Phys. Chem. A* **2000**, *104*, 8723−8729. (b) McClean, R. E. *J. Phys. Chem. A* **1999**, *103*, 75−79 and references therein. For the latter, see: (a) Rodriguez, J. A.; Dvorak, J.; Jirsak, T. *J. Phys. Chem. B* **2000**, *104*, 11515−11521. (b) Rodriguez, J. A.; Jirsak, T.; Pérez, M.; Chaturvedi, S.; Kuhn, M.; González, L.; Maiti, A. *J. Am. Chem. Soc.* **2000**, *122*, 12362−12370. (c) Rodriguez, J. A.; Hrbek, J. *Acc. Chem. Res.* **1999**, *32*, 719−728 and references therein.

(7) For an example of a thermodynamic study of the bonding between SO_2 and a well-defined transition metal complex, see: Albrecht, M.; Gossage, R. A.; Frey, U.; Ehlers, A. W.; Baerends, E. J.; Merbach, A. E.; van Koten, G. *Inorg. Chem.* **2001**, *40*, 850−855.

(8) Burshchka, C.; Baumann, F.-E.; Schenk, W. A. *Z. Anorg. Allg. Chem.* **1983**, *502*, 191−198.

(9) Ihmels, K.; Rehder, D. *Organometallics* **1985**, *4*, 1340−1347.

(10) Schenk, W. A.; Baumann, F.-E. *Chem. Ber.* **1982**, *115*, 2615−2625.

(11) Mews, R. *Angew. Chem., Int. Ed. Engl.* **1975**, *14*, 640.

(12) *Amsterdam Density Functional program*, version 2002.03; Division of Theoretical Chemistry, Vrije Universiteit: Amsterdam, The Netherlands; http://www.scm.com, 2002.

(13) (a) Baerends, E. J.; Ellis, D. E.; Ros, P. *Chem. Phys.* **1973**, *2*, 41−51. (b) Baerends, E. J.; Ros, P. *Chem. Phys.* **1973**, *2*, 52−59.

(14) Ravenek, W. In *Algorithms and Applications on Vector and Parallel Computers*; te Riele, H. J. J., Dekker, T. J., van de Horst, H. A., Eds.; Elsevier: Amsterdam, The Netherlands, 1987.

(15) (a) te Velde, G.; Baerends, E. J. *J. Comput. Chem.* **1992**, *99*, 84−98. (b) Boerrigter, P. M.; te Velde, G.; Baerends, E. J. *Int. J. Quantum Chem.* **1988**, *33*, 87−113.

(16) Versluis, L.; Ziegler, T. *J. Chem. Phys.* **1988**, *88*, 322−328.

(17) Vosko, S. H.; Wilk, L.; Nusair, M. *Can. J. Phys.* **1980**, *58*, 1200−1211.

(18) Perdew, J. P.; Chevary, J. A.; Vosko, S. H.; Jackson, K. A.; Pederson, M. R.; Singh, D. J.; Fiolhais, C. *Phys. Rev. B.* **1992**, *46*, 6671−6687.

(19) Van Lenthe, E.; van Leeuwen, R.; Baerends, E. J.; Snijders, J. G. *Int. J. Quantum Chem.* **1996**, *57*, 281.

(20) A reviewer asked for justification for not using diffuse functions for calculations involving anions. Diffuse functions unfortunately are not generally available in ADF basis sets.

(21) ADF Examples Manual for loss of CO from $Cr(CO)_6$, available from http://www.scm.com.

Table 1. Experimental and Predicted (PW91/TZP) Bond Distances (Å) for d^6 $(CO)_5M(SO_2)^{nq}$ Complexes

	S-bonded				O-bonded				η^2-SO-bonded						
	M−S	M−C_{ax}[a]	M−C_{eq}[a]	Δ_{M-C}[b]	M−O	M−C_{ax}[a]	M−C_{eq}[a]	Δ_{M-C}[b]	M−S	Δ_{M-S}[c]	M−O	Δ_{M-O}[c]	M−C_{ax}[a]	M−C_{eq}[a]	Δ_{M-C}[b]
Ti^{2-}	2.407	2.035	2.055 (1)	0.020	2.096	2.014	2.061 (24)	0.047	2.595	0.188	2.231	0.135	2.016	2.061	0.045
Zr^{2-}	2.591	2.206	2.237 (1)	0.031	2.223	2.192	2.231 (28)	0.039	2.732	0.143	2.331	0.108	2.199	2.237	0.038
Hf^{2-}	2.542	2.165	2.191 (1)	0.026	2.159	2.161	2.187 (34)	0.026	2.700	0.148	2.269	0.110	2.162	2.194	0.032
V^-	2.289	1.937	1.961 (1)	0.024	2.061	1.925	1.968 (4)	0.043	2.544	0.255	2.217	0.156	1.919	1.966	0.047
Nb^-	2.463	2.098	2.132 (1)	0.033	2.200	2.084	2.134 (3)	0.050	2.654	0.191	2.327	0.127	2.083	2.134	0.051
Ta^-	2.447	2.079	2.112 (1)	0.033	2.162	2.071	2.114 (4)	0.043	2.636	0.189	2.280	0.118	2.070	2.114	0.044
Cr	2.254	1.880	1.907 (1)	0.027	2.073	1.855	1.908 (1)	0.053	2.606	0.352	2.189	0.116	1.858	1.912	0.054
Cr	2.187	1.89	1.90 (expt)												
Mo	2.415	2.025	2.067 (1)	0.042	2.219	1.996	2.064 (1)	0.068	2.686	0.271	2.301	0.082	2.003	2.070	0.067
W	2.412	2.021	2.061 (1)	0.040	2.184	1.996	2.058 (1)	0.062	2.673	0.261	2.268	0.084	2.003	2.064	0.061

	S-bonded				O-bonded			
	M−S	M−C_{ax}[a]	M−C_{eq}[a]	Δ_{M-C}[b]	M−O	M−C_{ax}[a]	M−C_{eq}[a]	Δ_{M-C}[b]
Mn^+	2.274	1.854	1.884 (1)	0.030	2.093	1.824	1.882 (3)	0.058
Tc^+	2.421	1.985	2.034 (1)	0.049	2.240	1.946	2.028 (2)	0.082
Re^+	2.425	1.988	2.034 (1)	0.046	2.220	1.951	2.028 (2)	0.077
Fe^{2+}	2.341	1.863	1.889 (1)	0.026	2.050	1.836	1.888 (5)	0.052
Ru^{2+}	2.458	1.985	2.029 (1)	0.044	2.189	1.946	2.023 (3)	0.077
Os^{2+}	2.469	1.983	2.029 (1)	0.046	2.195	1.947	2.024 (5)	0.077

[a] M−C_{ax} is the metal−carbon bond distance for the carbonyl ligand trans to the SO_2 ligand. M−C_{eq} is the average of the four metal−carbon bond distances for the carbonyl ligands cis to the SO_2 ligand. The number in parentheses is the standard deviation of the values from the average. [b] Δ_{M-C} = [M−C_{eq} − M−C_{ax}] for a particular complex. [c] Δ_{M-S} = [M−S bond length in $(CO)_5M(\eta^2\text{-}SO_2)^{nq}$] − [M−S bond length in $(CO)_5M(\eta^1\text{-}SO_2)^{nq}$]. Δ_{M-O} = [M−O bond length in $(CO)_5M(\eta^2\text{-}SO_2)^{nq}$] − [M−O bond length in $(CO)_5M(\eta^1\text{-}OSO)^{nq}$].

Table 2. Experimental and Predicted (PW91/TZP) ν_{CO} and ν_{SO} Stretching Frequencies (cm^{-1}) for $(CO)_5M(SO_2)^{nq}$ Complexes

	ν_{CO}						ν_{SO}			
	expt	calcd	expt	calcd	expt	calcd	expt	calcd	expt	calcd
$(CO)_5V(\eta^1\text{-}SO_2)^-$	2018	1990	1940	1888	1895	1887		1194		1033
$(CO)_5Cr(\eta^1\text{-}SO_2)$	2101	2081	2012	1992	2006	1991	1311	1284	1117	1081
$(CO)_5Mo(\eta^1\text{-}SO_2)$	2107	2082	2009	1988		1986	1292	1283	1106	1078
$(CO)_5W(\eta^1\text{-}SO_2)$	2108	2081	2002	1985		1982	1292	1282	1105	1076
$(CO)_5Mn(\eta^1\text{-}SO_2)^+$	2167	2160	2061	2089	2040	2086	1311/1305	1358	1119	1112
$(CO)_5Mn(\eta^1\text{-}OSO)^+$		2149/2092		2066		2055		1257		1005
$(CO)_5Re(\eta^1\text{-}SO_2)^+$	2177	2172	2059	2079	2025	2079	1313/1307	1357	1114	1108
$(CO)_5Re(\eta^1\text{-}OSO)^+$		2152/2088		2059		2049		1258		993

Results and Discussion

A Note on Terminology. Because we will discuss the isomers separately and collectively, we adopt the following formula nomenclature. The S-bonded systems are represented by $(CO)_5M(\eta^1\text{-}SO_2)$, the O-bonded systems by $(CO)_5M(\eta^1\text{-}OSO)$, and the η^2-bonded systems as $(CO)_5M(\eta^2\text{-}SO_2)$. When no particular bonding mode is meant, we use generically $(CO)_5M(SO_2)$.

Structures and Conformational Energies. $(CO)_5M(\eta^1\text{-}SO_2)^{nq}$ Complexes. As already noted, this group contains the only structurally characterized example of a (pentacarbonyl)metal(SO_2) complex, $(CO)_5Cr(\eta^1$-planar $SO_2)$.[8] The theoretically predicted structure agrees reasonably well with experiment (Table 1). In particular, the model matches the Cr−C bond distances, and the rather small difference between the Cr−C_{ax} and Cr−C_{eq} values.[22] The model correctly predicts a planar SO_2 ligand, although it suggests a nearly perfectly staggered conformation for SO_2 with respect to the cis carbonyl ligands, while experiment finds an orientation closer to gauche (the smaller O−S−Cr−C_{eq} torsion angle is 29−35°). As we will discuss, this difference is probably irrelevant, since the SO_2 finds little barrier to rotation around the M−S axis. The Cr−S bond length displays the largest difference between model and experiment (2.254 vs 2.187 Å). However, the authors note[8] that this represents the shortest known Cr−S distance known in $(CO)_5CrL$ complexes by a wide margin (0.15−0.34 Å). Possibly a small amount of disorder artifactually shortened the experimental distance, or the short distance arises from solid state forces not modeled by the "gas phase" computation.

All the $(CO)_5M(\eta^1\text{-}SO_2)^{nq}$ complexes studied by IR spectroscopy have been characterized as containing S-bound η^1-planar SO_2. These assignments are consistent with the relative stabilities of the isomers (see the following bond energy data), except for the Mn^+ and Re^+ complexes, which the model predicts to be O-bonded. To confirm the utility of the model in predicting structures and physical properties, and to probe whether the structural assignment for the Mn^+ and Re^+ cations is tenable, we ran frequency calculations on those complexes for which experimental data exist. We compare these in Table 2. The experimental and theoretical data match well. In particular, the model correctly predicts the frequency trends for the series $(CO)_5V^-$/$(CO)_5Cr$/$(CO)_5Mn^+$, and the coincidence of the two lower energy

---

(22) C_{ax} (C_{axial}) is the carbonyl carbon trans to the SO_2 ligand; C_{eq} ($C_{equatorial}$) is used to represent an average value for the four COs cis to the SO_2 ligand.

Table 3. Hirschfeld Charges (PW91/TZP) for the Third-Row Transition Metal $(CO)_5M(SO_2)^{nq}$ Complexes

	SO_2	$(CO)_5Hf(SO_2)^{2-}$	$(CO)_5Ta(SO_2)^{-}$	$(CO)_5W(SO_2)$	$(CO)_5Re(SO_2)^{+}$	$(CO)_5Os(SO_2)^{2+}$
M		−0.037	0.016	0.063	0.121	0.194
C(trans)[a]		−0.037	0.023	0.087	0.151	0.216
C(cis)		−0.039	0.024	0.087	0.147	0.207
O(trans)		−0.245	−0.173	−0.096	-0.014	0.072
O(cis)		−0.237	−0.164	−0.086	−0.006	0.076
S	0.423	0.203	0.296	0.379	0.454	0.516
O	−0.212	−0.391	−0.302	−0.217	−0.138	−0.066

	$(CO)_5Hf(OSO)^{2-}$	$(CO)_5Ta(OSO)^{-}$	$(CO)_5W(OSO)$	$(CO)_5Re(OSO)^{+}$	$(CO)_5Os(OSO)^{2+}$
M	0.095	0.095	0.116	0.164	0.243
C(trans)	−0.038	−0.001	0.059	0.125	0.199
C(distcis)	−0.045	0.017	0.081	0.146	0.214
C(proxcis)	−0.025	0.022	0.077	0.136	0.201
O(trans)	−0.254	−0.191	−0.122	−0.042	0.052
O(distcis)	−0.244	−0.176	−0.101	−0.019	0.068
O(proxcis)	−0.226	−0.167	−0.099	−0.023	0.062
O(M)	−0.288	−0.210	−0.166	−0.145	−0.148
S	0.027	0.222	0.404	0.550	0.645
O	−0.460	−0.306	−0.206	−0.131	−0.080

	$(CO)_5Hf(\eta^2\text{-}SO_2)^{2-}$	$(CO)_5Ta(\eta^2\text{-}SO_2)^{-}$	$(CO)_5W(\eta^2\text{-}SO_2)$
M	0.047	0.069	0.110
C(trans)	−0.040	0.011	0.074
C(coplS)	−0.034	0.027	0.080
C(coplO)	−0.036	0.058	0.120
C(prox)	−0.004	0.028	0.085
C(dist)	−0.030	0.013	0.081
O(trans)	−0.254	−0.183	−0.105
O(coplS)	−0.241	−0.166	−0.094
O(coplO)	−0.244	−0.147	−0.071
O(prox)	−0.208	−0.161	−0.088
O(dist)	−0.240	−0.177	−0.094
O(M)	−0.345	−0.269	−0.214
S	0.071	0.228	0.349
O	−0.442	−0.329	−0.234

[a] Trans indicates an atom trans to SO_2, cis an atom cis to SO_2. Prox (proximal) indicates an atom that the SO_2 conformation points toward; dist (distal) indicates an atom that the SO_2 conformation points away from. O(M) is the SO_2 oxygen bound to the metal. CoplS and coplO apply only to the η^2-SO_2 bonding mode; the former indicates an atom coplanar with the metal−η^2-SO plane nearer the sulfur, and the latter indicates an atom nearer the oxygen.

Table 4. Predicted (PW91/TZP) Bond Dissociation Energy Data (kcal mol^{-1}) for $(CO)_5M(\eta^1\text{-}SO_2)^{nq}$, $(CO)_5M(\eta^1\text{-}OSO)^{nq}$, and $(CO)_5M(\eta^2\text{-}SO_2)^{nq}$ Complexes

	Ti^{2-}	Zr^{2-}	Hf^{2-}	V^{-}	Nb^{-}	Ta^{-}	Cr	Mo	W
$(CO)_5M{-}SO_2$	63.3	60.7	63.0	39.4	37.0	40.2	23.6	21.8	25.2
$(CO)_5M{-}OSO$	54.0	55.2	58.8	27.0	28.0	31.8	18.9	18.7	22.4
$(CO)_5M{-}(\eta^2\text{-}SO_2)$	64.6	65.7	69.3	36.0	38.0	41.8	18.6	20.3	24.1

	Mn^{+}	Tc^{+}	Re^{+}	Fe^{2+}	Ru^{2+}	Os^{2+}
$(CO)_5M{-}SO_2$	18.5	16.8	20.3	26.9	24.0	27.4
$(CO)_5M{-}OSO$	27.6	26.4	29.8	50.0	46.5	50.2

carbonyl stretches for $(CO)_5Mo(\eta^1\text{-}SO_2)$ and $(CO)_5W(\eta^1\text{-}SO_2)$. The S−O stretching frequencies are also well predicted. The latter strongly support the assignment of the $(CO)_5Mn^+$ and $(CO)_5Re^+$ complexes as being S-bound; the O-bound isomers should display bands at substantially lower energies than observed. Although this disagrees with the energetic data,[23] the overall general agreement between theoretical and experimental values for structures and vibrational frequencies supports the likelihood that the computational model accurately describes the structures of the uncharacterized complexes.

Several interesting trends/observations are apparent from examination of the predicted $(CO)_5M(\eta^1\text{-}SO_2)$ structures. Focusing on the SO_2 ligand first, we observe that in every case it adopts the η^1-planar conformation and a staggered orientation with respect to the cis carbonyl ligands. Figure 1a shows a view of $(CO)_5Mo(\eta^1\text{-}SO_2)$ demonstrating this. The η^1-planar conformation is that expected for SO_2 bound to a d^6 transition metal fragment from consideration of the interacting orbitals, and this implies the use of metal → SO_2 π-back-bonding.[5] Interestingly, optimized molecules where the SO_2 was constrained to the eclipsed position proved energetically very near their staggered counterparts. The two

---

(23) We employed a range of models (BP86, PW91, revPBE) and basis sets (DZ, TZP, TZ2P) within the ADF program and also using the Gaussian98 program (B3LYP/LANL2DZ.; B3LYP/LANL2DZ uncontracted on Re; 6-31G(d) on other atoms) to compare the energies of $(CO)_5Re(\eta^1\text{-}SO_2)^+$ and $(CO)_5Re(\eta^1\text{-}OSO)^+$. We also modeled the SO_2 solvent used to prepare $(CO)_5Mn/Re(SO_2)^+$ using the COSMO facility in the ADF program. All these approaches indicated that the η^1-OSO complex should be more stable than the η^1-SO_2 complex. We then compared the energies of these complexes including the AsF_6^- anion. While the η^1-OSO complex was still predicted to be of lower energy than the η^1-SO_2 isomer, the difference between the two was about half as large (from about 10−12 kcal mol^{-1} without the anion to about 6 kcal mol^{-1} with it). Also, a fluorine atom in the anion appears to interact strongly with the metal-bound sulfur in the η^1-SO_2 complex, but no (or little) such interaction arises in the η^1-OSO complex. We therefore postulate that the anion plays either a kinetic and/or a thermodynamic role in stabilizing the η^1-SO_2 isomer. This "counterion reversal" is unlikely to occur in the $(CO)_5M(SO_2)^{2+}$ complexes, where the energy difference between isomers is much larger, but it might be an issue for the anionic $(CO)_5M(SO_2)^-$ and $(CO)_5M(SO_2)^{2-}$ complexes. Evidently, it has no impact on the $(CO)_5V(SO_2)^-$ series, for which theory and experiment both predict a preference for the η^1-SO_2 isomer.

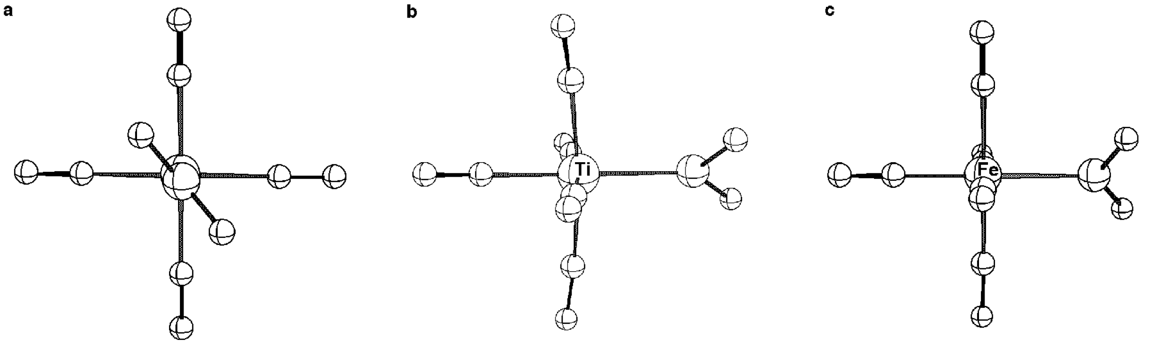

Figure 1. (a) View of the predicted (PW91/TZP) structure of $(CO)_5Mo(\eta^1\text{-}SO_2)$ down the S−Mo−C−O axis, showing the staggered conformation of the SO_2 ligand. (b) Side view of the predicted structure of $(CO)_5Ti(\eta^1\text{-}SO_2)^{2-}$. (c) Side view of the predicted structure of $(CO)_5Fe(\eta^1\text{-}SO_2)^{2+}$.

conformers typically showed energies differing by less than 1 kcal mol^{-1}. Eclipsed conformers transform smoothly to the staggered conformers during unconstrained optimizations, showing that essentially no barrier exists to rotation of the SO_2 fragment around the M−S axis. This is in accord with the molecular orbital pattern for a d^6 C_{4v}-$(CO)_5M$ fragment, where the filled d_{xz} and d_{yz} orbitals are degenerate and thus compete equally when back-bonding to the SO_2 ligand. The data suggest that at room temperature the SO_2 will “spin” readily, potentially blurring spectroscopic or diffraction experiments that rely on static atomic positioning. In particular, solid state single crystal X-ray diffraction studies might find the SO_2 moiety disordered; if not, the observed SO_2 conformation might reflect extraneous issues such as packing forces rather than a preference for that conformation. In this context, we note that *mer*-$Mo(CO)_3(\eta^1\text{-}SO_2)(P\text{−}{}^iPr_3)_2$ exhibits an eclipsed conformation with a very long Mo−S bond (2.285(3) Å),[24] while in the related *trans*-$Ru(NH_3)_4(\eta^1\text{-}SO_2)Cl^+$ and *trans*-$Ru(NH_3)_4(\eta^1\text{-}SO_2)(OH_2)^+$ the SO_2 adopts staggered and nearly staggered gauche orientations, respectively.[25]

Examining the carbonyl ligands second, we see that they bend away from the SO_2 ligand progressively as the negative charge increases. The extremes of the series of first-row molecules appear in Figure 1b,c to illustrate this. One sees that the plane containing the four carbonyls cis to the SO_2 ligand is essentially orthogonal to the M−S axis for the Fe^{2+} complex, but distortion increases across the series to the Ti^{2-} complex. The C_{ax}−M−C_{eq} angles average 90.0(1)° for Fe^{2+}, 89.4(1)° for Mn^+, 88.8(2)° for Cr, 88.2(2)° for V^-, and 86.5(6)° for Ti^{2-}.[26] These values are characteristic for each triad.

The origin of the repulsion lies in a sizable charge buildup on the sulfur-bound oxygens as the negative charge on the complex $(CO)_5M(\eta^1\text{-}SO_2)^{nq}$ increases from W to Ta^- to Hf^{2-}. Hirschfeld charges for the third-row systems appear in Table 3. One sees that, as the negative charge on the complex increases, the charges on all atoms decrease, but the change is greatest for the SO_2 moiety. The charge builds up most on the sulfur-bound oxygen atoms, so the carbonyls, although they repel each other, bend away from the SO_2 ligand and its greater negative charge. Conversely, as the positive charge increases, going from W to Re^+ to Os^{2+}, back-bonding decreases such that essentially no charge lies either on the carbonyl or on the sulfur-bound oxygens, so no repulsion exists and the carbonyls do not bend.

We note here that the enhanced negative charge on the sulfur oxygens as opposed to the carbonyl oxygens does not represent evidence that SO_2 is a better π-back-bonding ligand than is CO. Previous calculations and photoelectron spectroscopy indicate that the η^1-planar S-bonded SO_2 ligand acts as a better σ-donor than CO, but a poorer π-acceptor.[27] The vibrational calculations above support this, since we predict ν_{CO} for $(CO)_5W(\eta^1\text{-}SO_2)$, for example, to lie at higher energy (2081 cm^{-1}) than that for $W(CO)_6$ (2000 cm^{-1}). In addition, the M−C_{ax} bond distance in the $(CO)_5M(\eta^1\text{-}SO_2)$ species is always predicted to be shorter than the average M−C_{eq} distance. See Table 1. This is generally ascribed to the CO winning the competition for π-electron density over the ligand trans to it (in this case, SO_2). The ability of the sulfur oxygens to attract electrons probably arises from a combination of σ- and π-electron density transfers, some of which are unavailable to the carbonyl ligand.

Finally, the M−S bond lengths vary in an interesting way. The data are graphed in Figure 2. The trends down any particular triad are consistent with the relative sizes of the first-, second-, and third-row atoms/ions. However, one sees that the M−S bond lengths follow a u-shaped trend across a particular row, with the meniscus at the Cr/Mo/W triad. This mimics the behavior observed computationally for the M−C bond length in the d^6 series $M(CO)_6{}^q$ (M = Hf^{2-}−Ir^{3+}), where the meniscus lies around $Re(CO)_6{}^+/Os(CO)_6{}^{2+}$.[28] The trend relates to that predicted for the M−CO dissociation energy in that work, and with the M−SO_2 dissociation energy in ours. We therefore defer discussion to the bond dissociation energies subsection.

It is surprising to note that the η^1-SO_2 ligand adopts a planar orientation even in the dicationic complexes. One

---

(24) Kubas, G. J.; Jarvinen, G. D.; Ryan, R. R. *J. Am. Chem. Soc.* **1983**, *105*, 1883−1891.

(25) Kovalevsky, A. Y.; Bagley, K. A.; Coppens, P. *J. Am. Chem. Soc.* **2002**, *124*, 9241−9248.

(26) The number in parentheses is the standard deviation of the measurements from the mean.

(27) Schilling, B. E. R.; Hoffmann, R.; Lichtenberger, D. L. *J. Am. Chem. Soc.* **1979**, *101*, 585−591.

(28) (a) Diefenbach, A.; Bickelhaupt, F. M.; Frenking, G. *J. Am. Chem. Soc.* **2000**, *122*, 6449−6458. (b) Szilagyi, R.; Frenking, G. *Organometallics* **1997**, *16*, 4807−4815.

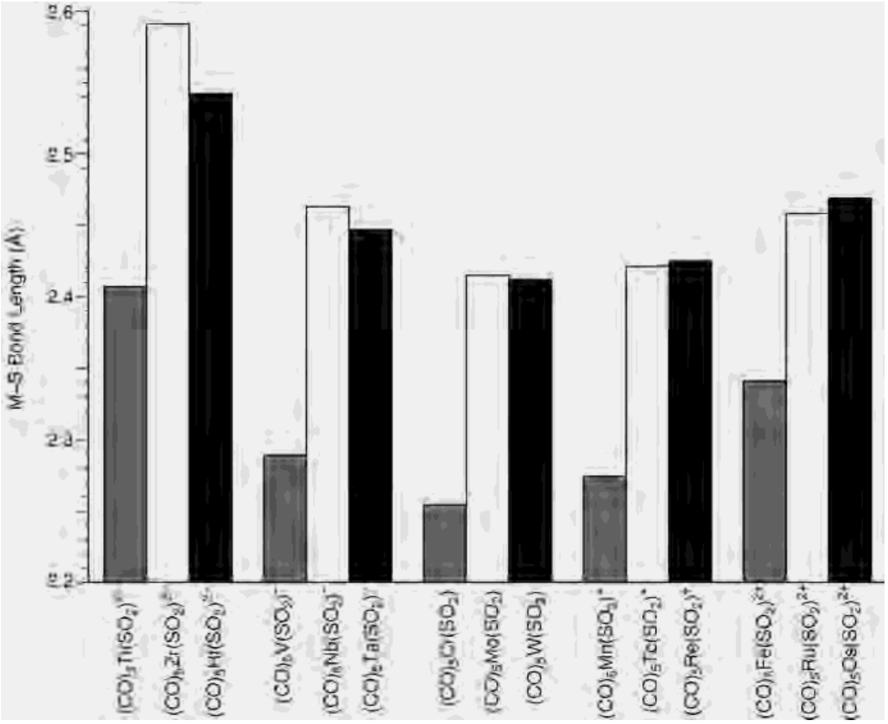

Figure 2. Predicted (PW91/TZP) M−S bond distances in d^6 $(CO)_5M(\eta^1\text{-}SO_2)^{nq}$ complexes compared by family and row.

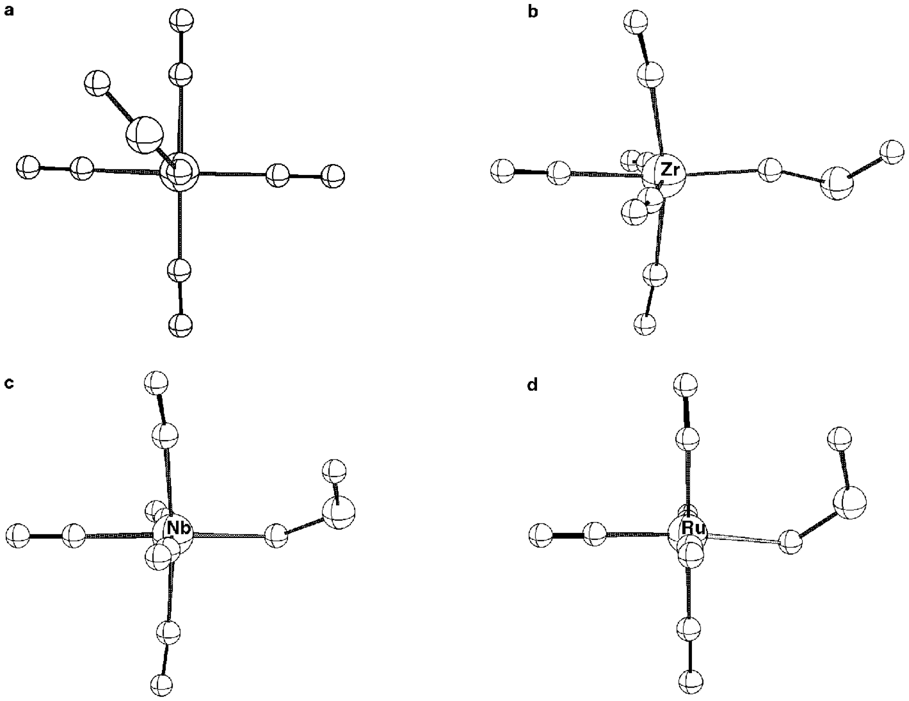

Figure 3. (a) View of the predicted (PW91/TZP) structure of $(CO)_5Mo(\eta^1\text{-}OSO)$ down the O−Mo−C−O axis, showing the staggered conformation of the OSO ligand. (b) Side view of the predicted structure of $(CO)_5Zr(\eta^1\text{-}OSO)^{2-}$. (c) Side view of the predicted structure of $(CO)_5Nb(\eta^1\text{-}OSO)^{-}$. (d) Side view of the predicted structure of $(CO)_5Ru(\eta^1\text{-}OSO)^{2+}$.

anticipates that π-back-bonding would be less important than σ-bonding for an electron-poor fragment such as $(CO)_5Fe^{2+}$, and thus that the η^1-SO_2 moiety should adopt a more pyramidal geometry. That it does not further substantiates the considerable π-back-bonding capacity of the η^1-SO_2 ligand, and the poor σ-donor ability of the sulfur atom. However, it also implies that use of pyramidality/planarity of the SO_2 ligand as a marker for the degree of electron richness of the metal fragment is not generally justified.

$(CO)_5M(\eta^1\text{-}OSO)^{nq}$ Complexes. Most of the trends discussed above for the S-bonded complexes apply to the O-bonded complexes as well. Figure 3a shows the archetype $(CO)_5Mo(\eta^1\text{-}OSO)$, which exhibits a bent u-shaped geometry for the SO_2 moiety rather than a bent z-shape or linear

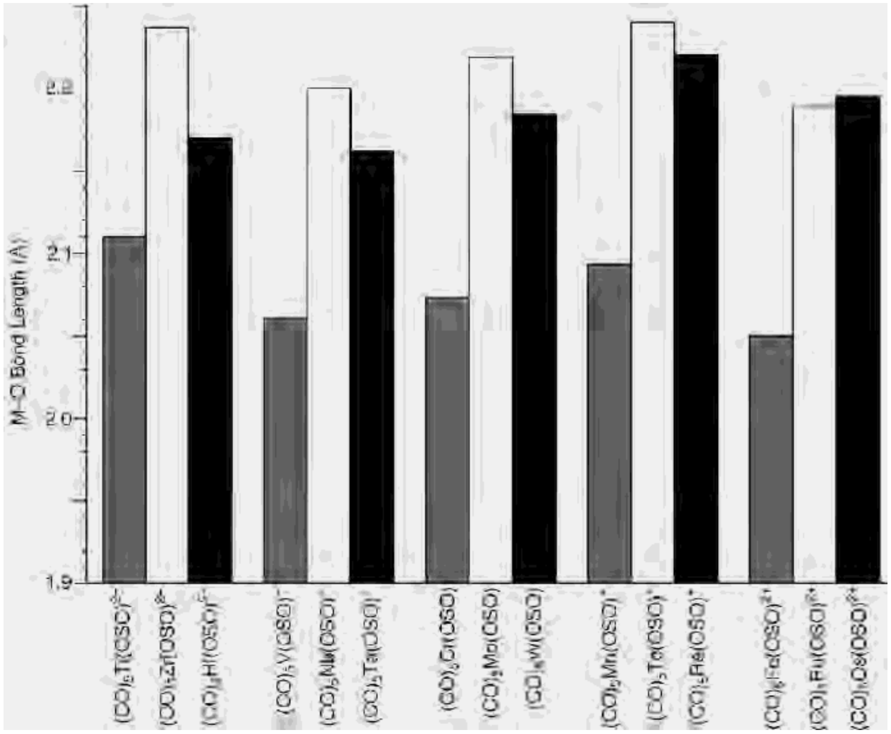

Figure 4. Predicted (PW91/TZP) M−O bond distances in d^6 $(CO)_5M(\eta^1\text{-OSO})^{nq}$ complexes compared by family and row.

versions of these. Since this choice elicits steric interactions with the carbonyl ligands, the OSO chain adopts a staggered conformation. However, the energetic difference between the staggered and eclipsed geometries remains small, on the order of 1 kcal mol^{-1}. We note that the staggered, bent u-shaped geometry is that found in the only structurally characterized example of an $L_5M(\eta^1\text{-OSO})$ complex (M = a transition metal), d^5 *trans*-$Mn(OPPh_3)_4(\eta^1\text{-OSO})_2^{2+}$, where both SO_2 ligands bind through the oxygen and adopt this conformation.[29] The Mn−O−S and O−S−O angles are 146.9(3)° and 116.2(4)°, respectively, in good agreement with the predicted values of 137.7° and 117.2°.

The exceptions to the general bonding motif arise in the $(CO)_5M(\eta^1\text{-OSO})^{2-}$ (M = Ti−Hf) series, the Zr example of which appears in Figure 3b. The OSO chain in these complexes exhibits the eclipsed bent-z conformation. In all three, the carbonyl ligands distort significantly, as shown. We have not been able to correlate this structure with any idealized six-coordinate geometry. Since these complexes contain the most electron-rich (pentacarbonyl)metal fragments, the selection of this conformer suggests either that the eclipsed z-orientation maximizes the ability of the OSO chain to act as a π-acid, or that it minimizes the σ-donor capacity of the oxygen atom. Probably both issues play some role. Unfortunately, the Hirschfeld charge data (Table 3) do not assist in distinguishing the two. One sees that the charges on all atoms decrease as the overall charge does from W to Ta^- to Hf^{2-}. The sole exception is the Hf atom itself, which the model predicts to carry the same charge as the Ta atom in the monoanionic analogue. This suggests that the Hf donates more electron density to the ligands because of the structural change, but whether more density goes to the SO_2 or to the carbonyls is difficult to determine.

As above, the carbonyl ligands bend away from the SO_2 ligand progressively as the negative charge increases. A series of second-row complexes appears in Figure 3b−d to illustrate this. The $C_{ax}-M-C_{eq}$ angles average 90.6(4)° for Ru^{2+}, 89.9(3)° for Tc^+, 88.6(2)° for Mo, 86.6(5)° for Nb^-, and 83(3)° for Zr^{2-}. These values are characteristic for each triad. Comparing these data with those for the S-bonded complexes shows that the cationic and neutral species exhibit essentially the same degree of bending regardless of what atom is bonded, but the electron-rich anionic complexes display greater bending when the SO_2 is O bonded. This supports the idea that O-bonded SO_2 is a poorer π-acid than is S-bonded SO_2.

Also as already described, the model always predicts the $M-C_{ax}$ bond distance to be shorter than the average $M-C_{eq}$ distance. See Table 1. The difference Δ_{M-C} is consistently larger than for the S-bonded complexes. This result, plus the observation that carbonyl bending occurs to a greater extent for O-bonded systems, supports the intuitive view that oxygen is a better σ-donor than is sulfur and that the O-bonded OSO chain is a poorer π-acid than the S-bonded SO_2 ligand.

The M−O bond lengths also generally follow a u-shaped trend across a particular row, with the meniscus at the V/Nb/Ta triad. However, the curve is not as concave as that already observed, and as is evident, the Fe triad complexes break the pattern by showing short M−O distances (Figure 4). Only this last observation correlates well with the M−O bond energies (see in a following subsection). In general, the M−O bond distance cannot be used to predict the bond energy in these systems.[30]

---

(29) Gott, G. A.; Fawcett, J.; McAuliffe, C. A.; Russell, D. R. *J. Chem. Soc., Chem. Commun.* **1984**, 1283−1284.

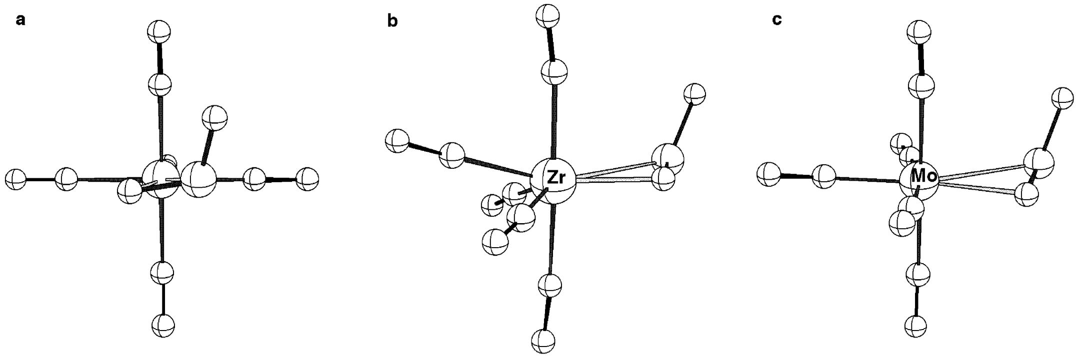

Figure 5. (a) View of the predicted (PW91/TZP) structure of $(CO)_5Mo(\eta^2\text{-}SO_2)$ down the $(\eta^2\text{-}SO)-Mo-C-O$ axis, showing the eclipsed conformation and facial bonding of the η^2-SO_2 ligand. (b) Side view of the predicted structure of $(CO)_5Zr(\eta^2\text{-}SO_2)^{2-}$. (c) Side view of the predicted structure of $(CO)_5Mo(\eta^2\text{-}SO_2)$.

$(CO)_5M$-$(\eta^2\text{-}SO_2)^{nq}$ Complexes. A number of η^2-SO_2 complexes have appeared in the literature. In general, they require a moderately electron-rich metal center, such as in the d^6 complexes $Mo(CO)_3(phen)(\eta^2\text{-}SO_2)$[31] or *trans*-$Ru(NH_3)_4Cl(\eta^2\text{-}SO_2)^+$.[25] Our calculations confirm this view, in that we found that attempts to optimize cationic $(CO)_5M(\eta^2\text{-}SO_2)^{n+}$ complexes invariably led to rearrangement to form O-bonded $(CO)_5M(\eta^1\text{-}OSO)^{n+}$ complexes. This illustrates the analogy between the η^2-SO_2 ligand and the η^2-alkene ligand, where both σ-donation and π-acidity are required for strong bonding. The cationic (pentacarbonyl)metal fragments are poorer π-bases, so the η^2-bonding is weaker. The oxygen atom of the ligand presents the hard, cationic metal with a hard base to bind, at the expense of dissociating the softer sulfur atom. Hirschfeld charge data (Table 3) provide some support for this idea. One sees that the sulfur atom increases its positive charge rapidly as the positive charge on the complex increases, a total of 0.28 e^- from Hf to W. By contrast, the charge on the metal-bound oxygen increases more slowly, a total of 0.13 e^-.

Representative examples of the η^2-SO_2 complexes appear in Figure 5. One sees that the metal binds to the "face" of the SO_2 ligand, so that the plane containing the SO_2 lies parallel to that containing the four cis carbonyl ligands. This confirms the view that η^2-SO_2 binds like an η^2-alkene.[24] The usual distortion of the carbonyl ligands is observed as the anionic charge on the metal fragment increases (Figure 5b,c), becoming extreme for the dianionic $(CO)_5M(\eta^2\text{-}SO_2)^{2-}$ complexes. As already observed, the $M-C_{ax}$ distance is shorter than the $M-C_{eq}$ distance (Table 1), indicating that even when η^2-bound, the SO_2 ligand is a better donor than is CO.

In contrast to the staggered conformation adopted by the η^1 complexes already described, the η^2-SO_2 ligand prefers an eclipsed orientation, as shown in Figure 5a. This agrees with experimental observations for a number of d^6 metal$-(\eta^2\text{-}SO_2)$ species.[5] As described, we find that the energetic difference between staggered and eclipsed conformations is not large (1$-$2 kcal mol^{-1}), and rotation of the S$-$O vector with respect to the $(CO)_5M$ fragment appears barrierless. It is thus unsurprising that a few examples of molecules containing a staggered η^2-SO_2 exist.[5]

One sees in Table 1 that Δ_{M-S}, the difference between the M$-$S bond length in the η^2-SO_2 complexes and the M$-$S bond length in the $M(\eta^1\text{-}SO_2)$ complexes, is substantially larger than the analogous Δ_{M-O}. The difference increases from the dianions to the neutral complexes, correlating with the fact that when the metal fragment carries a positive charge, the sulfur does not coordinate. Figure 6 shows that the M$-$S bond lengths follow a u-shaped pattern with the meniscus at the V triad, while the M$-$O distances do not exhibit any apparent trend.

$(CO)_5M(SO_2)$ Bond Dissociation Energies. Figure 7 shows graphically the bond dissociation energies (BDEs) for the η^1-SO_2, η^1-OSO, and η^2-SO_2-bonded complexes; numerical values appear in Table 4. The BDEs track the relative stabilities of the isomers, so we will treat the two interchangeably here.

In keeping with the predictions and experimental data for the M$-$CO BDEs for $M(CO)_6{}^{nq}$ complexes,[32] the M$-$S and M$-$O BDEs generally display a u-shaped trend down a family. The u-shape reflects the competition between orbital overlap (better for first-row metals) and relativistic effects (better for third-row metals).[33] The range between the three in a particular family is not large, finding a maximum of ca. 5 kcal mol^{-1} for the $(CO)_5(Ti-Hf)(\eta^1\text{-}OSO)^{2-}$ series, but typically less than half this value. In contrast, the BDEs for the η^2-SO_2 complexes rise smoothly down the family, although again the range spanned is small. Solely on the basis of these data, it appears that first-row catalysts for SO_2 reactions should prove as effective as more-expensive second- and third-row catalysts.

The u-shaped trend across a row noted above for bond lengths occurs here as well. The largest BDEs appear for the dianions in the titanium family, reaching the remarkable

---

[30] Frenking, G.; Wichmann, K.; Fröhlich, N.; Grobe, J.; Golla, W.; Le Van, D.; Krebs, B.; Läge, M. *Organometallics* **2002**, *21*, 2921$-$2930.

[31] Kubas, G. J.; Ryan, R. R.; McCarty, V. *Inorg. Chem.* **1980**, *19*, 3003$-$3007.

[32] (a) Ziegler, T. *Can. J. Chem.* **1995**, *73*, 743$-$761 and references therein. (b) Ziegler, T. *Chem. Rev.* **1991**, *91*, 651$-$667 and references therein.

[33] Ziegler has given a cogent explanation of how relativity strengthens metal$-$ligand bonds through back-donation to the ligand. See ref 32a and see: Ziegler, T. In *Metal$-$Ligand Interactions: from Atoms to Clusters to Surfaces*; Salahub, D. R., Russo, N., Eds.; Kluwer: The Netherlands, 1992, 367$-$396.

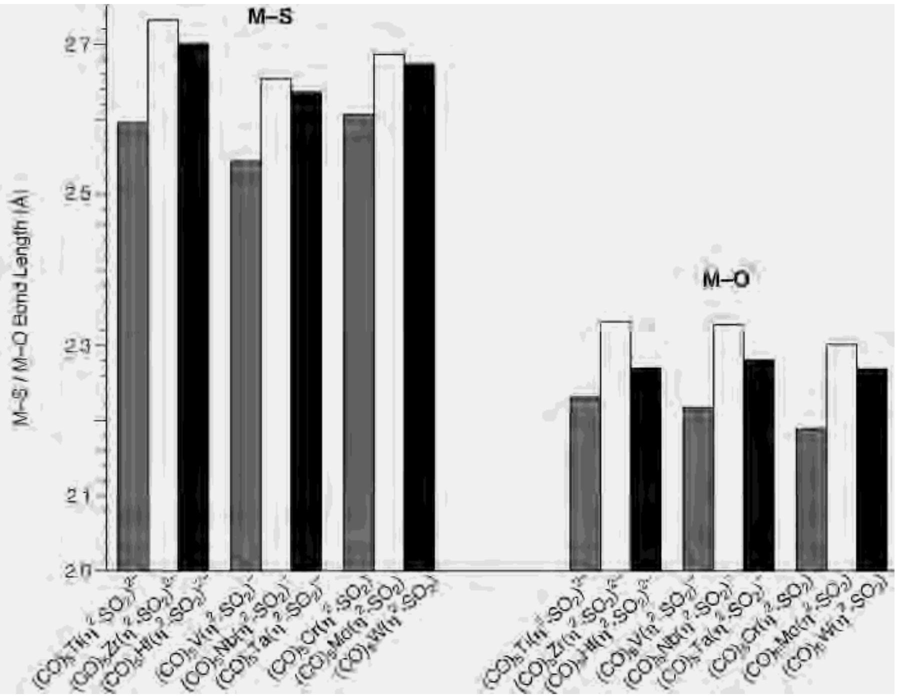

Figure 6. Predicted (PW91/TZP) M−S and M−O bond distances in d^6 $(CO)_5M(\eta^2\text{-}SO_2)^{nq}$ complexes compared by family and row.

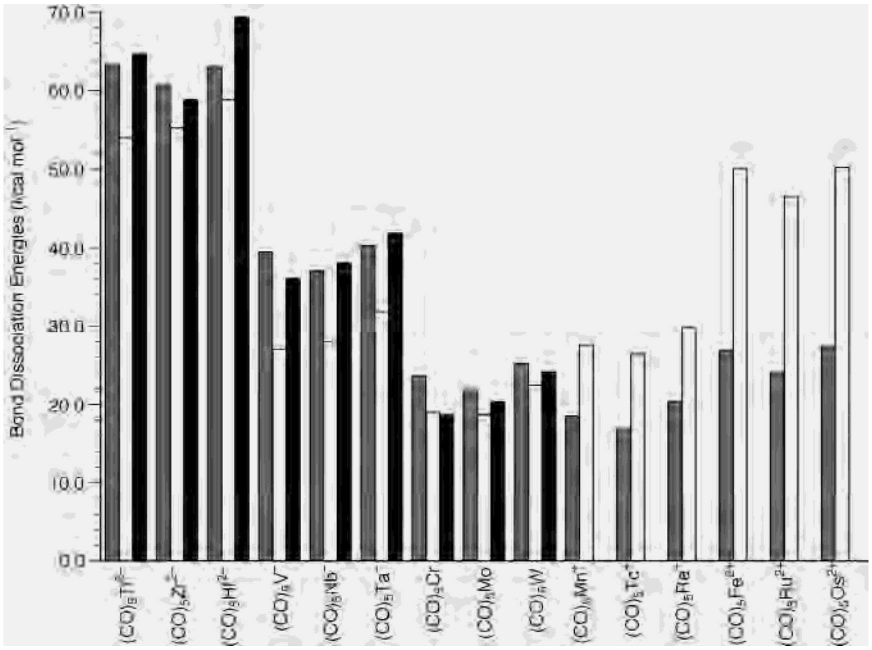

Figure 7. Predicted (PW91/TZP) bond dissociation energies (BDEs) (kcal mol^{-1}) for all complexes studied. Gray columns correspond to the energy for $(CO)_5M(\eta^1\text{-}SO_2)^{nq} \rightarrow (CO)_5M^{nq} + SO_2$, white columns correspond to the energy for $(CO)_5M(\eta^1\text{-}OSO)^{nq} \rightarrow (CO)_5M^{nq} + SO_2$, and black columns correspond to the energy for $(CO)_5M(\eta^2\text{-}SO_2)^{nq} \rightarrow (CO)_5M^{nq} + SO_2$.

values of 65−70 kcal mol^{-1} for the $(CO)_5M(\eta^2\text{-}SO_2)^{2-}$ complexes. Surprisingly, even the (presumably) less π-accepting η^1-SO_2 and η^1-OSO bonding motifs still exhibit sizable BDEs here. The fact that the η^2-SO_2 complexes show the largest BDEs speaks to the need for extensive M → SO_2 back-bonding in these electron-rich ions. The substantial BDEs even with the S-bound and O-bound anions argue that these motifs involve π-back-bonding also, as already suggested. For the M−S and M−O BDEs (for which full sets of predictions were possible), the meniscus for the former occurs at the manganese family, while that for the latter occurs at the chromium family, with BDEs of ca. 20 kcal mol^{-1}, regardless of how the SO_2 ligand binds. Since $(CO)_5$-(Cr−W)(η^1-SO_2) and $(CO)_5$(Mn, Re)$(\eta^1\text{-}SO_2)^+$ complexes exist, this implies that most of the other d^6 complexes should prove preparable and more stable. We hope this work will spur experimentalists to expand beyond this limited complex set.

The model suggests an array of experiments to pursue. For example, it correctly predicts the observed preference for S-bonding for the neutral $(CO)_5$(Cr−W)(SO_2) complexes. However, the preference is slight, particularly for tungsten, so careful experiments might allow isolation or observation of the η^1-OSO and η^2-SO_2 isomers. In this regard, we note that Coppens et al. showed that *trans*-Ru$(NH_3)_4$Cl$(\eta^1\text{-}SO_2)^+$ converts to *trans*-Ru$(NH_3)_4$Cl$(\eta^2\text{-}SO_2)^+$ when irradiated in the crystalline state.[25] By contrast, the model incorrectly predicts that the series $(CO)_5(Mn{-}Re)(\eta^1\text{-}OSO)^+$ should be more stable than the experimentally observed η^1-SO_2 isomers.[23] Possibly the latter are kinetic products, and another synthetic approach (possibly involving a less coordinating anion) would provide the former as thermodynamic products. In this same vein, the model predicts far greater stability for the O-bound isomer versus the S-bound isomer for the dicationic $(CO)_5(Fe{-}Os)(SO_2)^{2+}$ series; it would be interesting to see if experiment bears this out. On the other side of the BDE meniscus, the model correctly predicts that $(CO)_5V(\eta^1\text{-}SO_2)^-$ is more stable than the alternatives, but it indicates that the niobium and tantalum analogues should prefer the η^2-SO_2 motif. If borne out by experiment, this distinction would provide insight into a subtle relationship between metal basicity and bonding mode.

The u-shaped trend itself is interesting. Qualitatively, one explains it as a competition between two bonding effects. For the anionic species on the left side of the scale, M → SO_2 π-back-bonding dominates, so that the greater the electron density on the metal, the stronger the bond. Proceeding to the right, and greater positive charge, the metal becomes more Lewis acidic and harder in hard−soft acid−base terms, so that bonding becomes more ionic in nature, increasing the BDE. This conforms to the prediction that O-bonded complexes are particularly stable for the cations, since oxygen is a hard base, while the S-bonded complexes are more stable for the neutrals and anions, since sulfur is a soft base.

Quantitatively, we examined the bonding using the energy decomposition data available in ADF output. The approach has been described in several places,[28,30,32,33] so we discuss it only briefly. The BDE is decomposed to terms as follows:

$$\Delta E_{\mathrm{BDE}} = \Delta E_{\mathrm{prep}} + \Delta E_{\mathrm{int}} = \Delta E_{\mathrm{prep}} + \Delta E_{\mathrm{elstat}} + \Delta E_{\mathrm{Pauli}} + \Delta E_{\mathrm{orb}}$$

where ΔE_{prep} is the energy associated with deforming the fragments of interest to their geometries in the molecule/ion, $\Delta E_{\mathrm{elstat}}$ is the electrostatic interaction energy between the fragments, $\Delta E_{\mathrm{Pauli}}$ is the repulsive interaction energy between the fragments resulting from interactions between occupied orbitals, and ΔE_{orb} is the energy associated with relaxation of the Kohn−Sham orbitals as self-consistency is reached. $\Delta E_{\mathrm{elstat}}$ and ΔE_{orb} broadly describe electrostatic and covalent attractive aspects of bonding, respectively, while $\Delta E_{\mathrm{Pauli}}$ describes repulsive aspects. For the systems here, ΔE_{prep} is generally on the order of 3 kcal mol^{-1}, although it rises to ca. 10 kcal mol^{-1} for highly distorted species such as $(CO)_5(Ti{-}Hf)(\eta^1\text{-}OSO)^{2-}$. However, its contribution to the overall BDE is limited, so here we focus on the components of ΔE_{int}. These have more effect on the bond energy trends already noted.

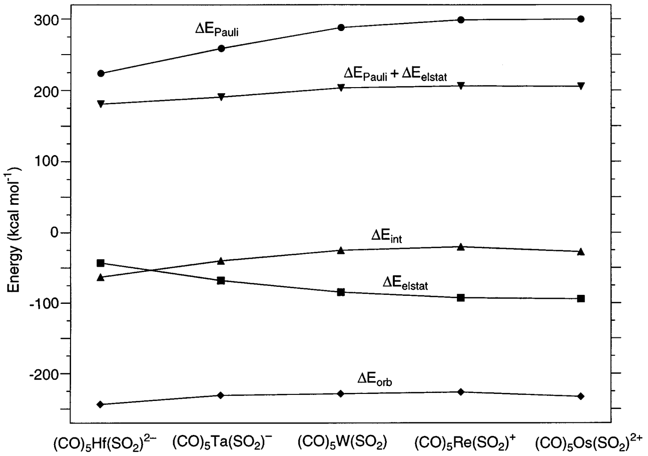

Figure 8. Relative energies (PW91/TZP, kcal mol^{-1}) of the terms in the bond energy decomposition for the third-row transition metal reactions $(CO)_5M(\eta^1\text{-}SO_2)^{nq} \rightarrow (CO)_5M^{nq} + SO_2$.

As representative of the $(CO)_5M(\eta^1\text{-}SO_2)^{nq}$ complexes, Figure 8 gives a graph of the components of ΔE_{int} for the third-row metal complexes $(CO)_5M(\eta^1\text{-}SO_2)$. One sees that the three components are energetically well separated. In contrast to the situation for the hexa(carbonyl)metal complexes studied by Frenking et al.,[28] $\Delta E_{\mathrm{elstat}}$ does not cross ΔE_{orb} at any point. The repulsive $\Delta E_{\mathrm{Pauli}}$ rises fairly smoothly from Hf to W, and then flattens, changing overall by ca. 75 kcal mol^{-1}. One interprets this as showing that, as the filled orbitals are pulled more closely to the nucleus by the increasing positive charge, the Pauli repulsion increases, and that repulsion becomes asymptotic. By contrast, $\Delta E_{\mathrm{elstat}}$ decreases asymptotically by ca. 50 kcal mol^{-1}; the electrostatic attraction between fragments increases as the positive charge on the metal increases. At the same time, ΔE_{orb} remains nearly constant across the series, changing by only ca. 15 kcal mol^{-1} (and by only 6 kcal mol^{-1} from Ta to Os), peaking at W. Thus, the u shape of the ΔE_{int} curve is determined largely by the sum of the factors, $\Delta E_{\mathrm{Pauli}} + \Delta E_{\mathrm{elstat}}$, with a small contribution from ΔE_{orb}. We note that the sum, $\Delta E_{\mathrm{Pauli}} + \Delta E_{\mathrm{elstat}}$, is often termed $\Delta E_{\mathrm{steric}}$ or $\Delta E°$, to contrast it with the covalent term, ΔE_{orb}. In this language, the shape of the BDE curve arises from the steric term.

The BDE decomposition data for the oxygen-bound $(CO)_5M(\eta^1\text{-}OSO)^{nq}$ species are less straightforward (Figure 9). One sees, for example, that $\Delta E_{\mathrm{elstat}}$, and $\Delta E_{\mathrm{Pauli}}$ cross going from Hf to Ta, and that both curves change nearly linearly, and then flatten dramatically at Re. $\Delta E_{\mathrm{Pauli}}$ is predicted to be attractive for Hf, while the model predicts $\Delta E_{\mathrm{elstat}}$ to be repulsive for Hf and Ta. Both observations reflect the repulsion between the compact, filled oxygen lone pair orbitals and the anionic metal fragment; the attractive $\Delta E_{\mathrm{Pauli}}$ implies “spreading” of the filled orbitals and thus decreased pair−pair interactions.

Moreover, ΔE_{orb} changes significantly over the series, in contrast to the η^1-SO_2 systems already described. The behavior here mimics that analyzed by Frenking and coworkers for the related d^6 $(CO)_5M{-}CO^{nq}$ (M = Hf−Ir; *nq* = 2− to 3+) BDEs.[28] They quantified the qualitatively

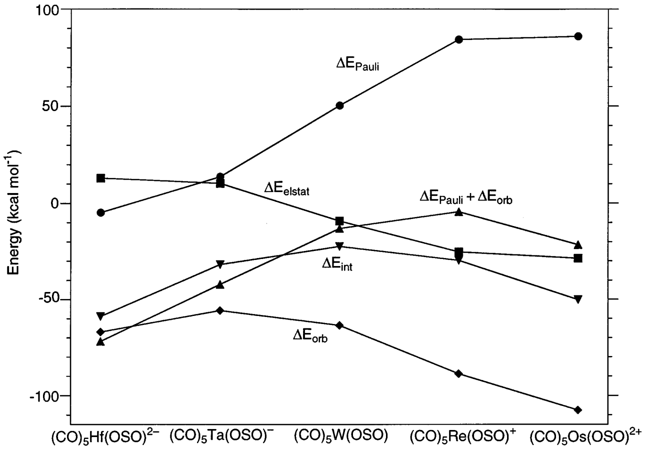

Figure 9. Relative energies (PW91/TZP, kcal mol^{-1}) of the terms in the bond energy decomposition for the third-row transition metal reactions $(CO)_5M(\eta^1\text{-OSO})^{nq} \rightarrow (CO)_5M^{nq} + SO_2$.

expected result that M → CO π-back-bonding contributed most to the BDE for the Hf^{2-}, Ta^-, and W complexes, while OC → M σ-donation dominated for the cationic Re^+, Os^{2+}, and Ir^{3+} complexes. This ties to the high-lying HOMOs and LUMOs for the former three $(CO)_5M^{nq}$ fragments and the low-lying HOMOs and LUMOs for the latter three fragments. They further found that orbital energy match was more important than orbital overlap. On the basis of orbital energy match, one expects improved bonding between low energy oxygen orbitals on SO_2 and the low-lying orbitals of the cationic fragments, and this holds for ΔE_{orb} here.

As a result, all three factors as a group determine the u-shape of the ΔE_{int} curve; no two dominate. By way of demonstration, we plotted the curve for $\Delta E_{Pauli} + \Delta E_{orb}$ in Figure 9. One sees that it peaks at Re; this holds for the other possible data pairs as well. The shift of the curve from the true meniscus at W shows that each term contributes importantly to the overall ΔE_{int}.

The η^2-SO_2 complexes represent an interesting spread of behavior across rows, being substantially the most stable isomer for the dianionic complexes, but decreasing rapidly in relative stability until being predicted not to exist for the mono- and dications. At no point is the BDE for an η^2-SO_2 complex anywhere near as large as the sum of the M−S and M−O BDEs. This correlates with the prediction that the M−S and M−O bond distances for any $(CO)_5M(\eta^2\text{-}SO_2)$ complex are substantially longer than the corresponding distances in the $(CO)_5M(\eta^1\text{-}SO_2)$ and $(CO)_5M(\eta^1\text{-OSO})$ isomers; the added bonding potentially created by coordinating both atoms is negated by weaker interactions between the atoms and the metal.

We show in Figure 10 the bond decomposition data for the third-row (η^2-SO_2) complexes. Since two members of the set are missing, interpretation of the data is speculative. The model suggests that ΔE_{elstat} contributes less to the BDE trend, changing only 15 kcal mol^{-1} over the three. By contrast, ΔE_{Pauli} and ΔE_{orb} change by 24 and 37 kcal mol^{-1}, respectively. This makes sense given the described results, since ΔE_{elstat} contributes most to ΔE_{int} trends for neutrals and cations. That ΔE_{orb} changes the most indicates that these are the most covalent of the three systems, which supports the bonding picture for η^2-SO_2 being similar to that for η^2-alkenes.

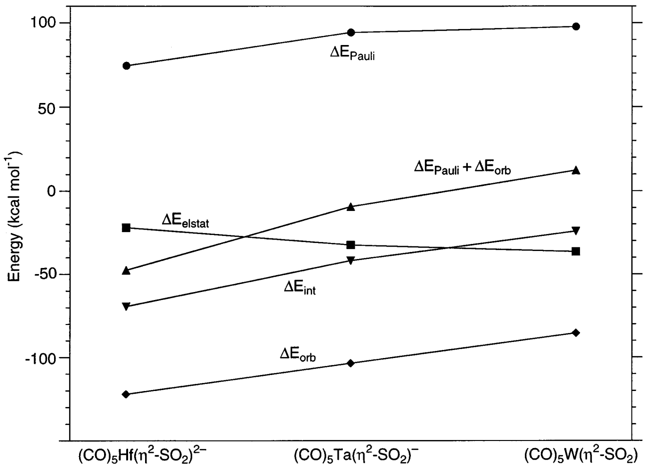

Figure 10. Relative energies (PW91/TZP, kcal mol^{-1}) of the terms in the bond energy decomposition for the third-row transition metal reactions $(CO)_5M(\eta^2\text{-}SO_2)^{nq} \rightarrow (CO)_5M^{nq} + SO_2$.

Conclusions

The computational model performs well in predicting the structures and vibrational spectra of the various isomers of $(CO)_5M(SO_2)^{nq}$, and so probably models the BDEs reasonably. The results suggest that a number of as yet unsynthesized complexes should prove to be readily prepared. For example, the BDEs of the series $(CO)_5(Ti{-}Hf)(\eta^2\text{-}SO_2)^{2-}$ are so large that the approaches pioneered by Ellis should provide them.[34]

The model suggests that one should think of SO_2 as a ligand similar to CO: a poor σ-donor and strong π-back-bonder. This applies best to the η^1-SO_2 and η^2-SO_2 bonding motifs. The bond energy decomposition data indicate that, within the bonding picture, electrostatics determine the shape of the energy trend curve for the former, while covalency determines the shape for the latter. The two tend to match for a particular complex, so that the BDEs for the two isomers are similar. The η^1-OSO bonding motif exhibits less straightforward behavior in its bonding details, but the qualitative message is obvious: these will be most stable (and more stable than the other isomers) when the metal fragment is a hard Lewis acid, e.g., cationic.

Finally, the data provide some perspective in designing catalysts for converting SO_2 into innocuous materials. Clearly, SO_2 binds most strongly to very electron-rich metal systems, so electron-richness represents a plausible design criterion for a good catalyst for immobilizing SO_2. However, the strong binding may limit further reactivity. In this regard, we note that the electron-poor dications bind SO_2 reasonably well through the oxygen atom. We suggest that a heteronuclear catalyst, containing adjacent electron-rich and electron-poor binding sites, will secure both ends of the SO_2 molecule,

---

(34) (a) Jang, M.; Ellis, J. E. *Angew. Chem., Int. Ed. Engl.* **1994**, *33*, 1973−1975. (b) Ellis, J. E.; Chi, K.-M. *J. Am. Chem. Soc.* **1990**, *112*, 6022−6025.

thereby immobilizing it and activating it toward further chemistry.

Acknowledgment. We thank Drs. Greg Kubas (LANL) and Ken Caulton (Indiana University) for helpful discussions. The NIU Computational Chemistry Laboratory (NIU CCL) is supported in part by the taxpayers of the State of Illinois. H.J.R. was supported by the NIU Undergraduate Research and Artistry Program (URAP).

Supporting Information Available: Optimized Cartesian coordinates and energies of the molecules/ions examined in this study. This material is available free of charge via the Internet at http://pubs.acs.org.

IC030179P